Received: 13 February 2022 | Revised: 18 March 2022 | Accepted: 19 March 2022

DOI: 10.1002/htj.22530

RESEARCH ARTICLE

HEAT TRANSFER WILEY

Magnetoconvection around an elliptic cylinder placed in a lid-driven square enclosure subjected to internal heat generation or absorption

Olalekan A. Olayemi[1,2] | **Khaled Al-Farhany**[3] | **Adebowale M. Obalalu**[4] | **Tomisin F. Ajide**[1] | **Kehinde R. Adebayo**[5]

[1]Department of Aeronautics and Astronautics, Faculty of Engineering and Technology, Kwara State University, Malete, Kwara, Nigeria

[2]School of Engineering, Cranfield University, Cranfield, UK

[3]Department of Mechanical Engineering, University of Al-Qadisiyah, Al Diwaniyah, Iraq

[4]Department of Physics, Augustine University Ilara-Epe, Epe, Lagos, Nigeria

[5]Department of Food and Agricultural Engineering, Kwara State University, Malete, Kwara, Nigeria

Correspondence
Khaled Al-Farhany, Department of Mechanical Engineering, University of Al-Qadisiyah, Al Diwaniyah 58001, Iraq.
Email: khaled.alfarhany@qu.edu.iq

Olalekan A. Olayemi, Department of Aeronautics and Astronautics, Faculty of Engineering and Technology, Kwara State University, Malete, Kwara, Nigeria.
Email: olalekan.olayemi@kwasu.edu.ng and olalekan.a.olayemi@cranfied.ac.uk

Abstract

The impacts of MHD and heat generation/absorption on lid-driven convective fluid flow occasioned by a lid-driven square enclosure housing an elliptic cylinder have been investigated numerically. The elliptic cylinder and the horizontal enclosure boundaries were insulated and the left vertical lid-driven wall was experienced at a fixed hot temperature, and the right wall was exposed to a fixed cold temperature. COMSOL Multiphysics 5.6 software was used to resolve the nondimensional equations governing flow physics. A set of parameters, such as Hartmann number ($0 \leq Ha \leq 50$), Reynolds number ($10^2 \leq Re \leq 10^3$), Grashof number ($10^2 \leq Gr \leq 10^5$), heat generation-absorption parameter ($-3 \leq J \leq 3$), and elliptical cylinder aspect ratio (AR) ($1.0 \leq AR \leq 3.0$) have been investigated. The current study discovered that for low Reynolds number, the adiabatic cylinder AR of 2.0 provided the optimum heat transfer enhancement for the model investigated, also the impact of cylinder size diminishes beyond $Gr = 10^4$. But for high Reynolds ($Re = 1000$), the size of the cylinder with AR = 3.0 offered the highest heat transfer augmentation. The clockwise flow circulation

 © 2022 Wiley Periodicals LLC

reduces because of an increase in AR, which hinders the flow circulation. In addition, heat absorption supports heat transfer augmentation while heat generation can suppress heat transfer improvement.

KEYWORDS
absorption, elliptic cylinder, Hartmann number, heat generation, magnetoconvection

1 | INTRODUCTION

Mixed convection in enclosures of various configurations has captured numerous researchers' interest over the years owing to its broad technological engagements, such as in the cooling of electronic devices, nuclear reactors, chemical processing equipment, lubricating groves, and in the manufacturing of float glass and coating. Some of the previous works done on mixed convective heat transfer are captured in various studies.[1–6] Olayemi et al.[7] considered lid-driven convective flow in a square cavity exposed to different modes of heating and submitted that the maximum heat transfer took place close to the lower wall and the highest value of flow velocity occurrence at $y = 0.4$ in the vertical midplane at $x = 0.5$. Khan et al.[8] analyzed lid-driven convective flow in a trapezoidal configuration housing a cylinder that was subjected to rotary motion. Reports from the analysis show that for large wall orientation angle when the Grashof number is lowered the heat transfer rate decreases. Yang and Farouk[9] researched mixed convective flow in a circular domain equipped with a heated rotating square cylinder. The report opined that as the inner-to-outer cylinder ratio increases, *Nu* decreases. Chamkha et al.[10] reported studies on the inner rotary motion that occurred in a porous cavity. According to their findings, the average and local heat transfer coefficients rise when the cylinder approaches either the upper or lower regions of the domain considered.

Olayemi et al.[11] considered buoyancy-dependent flow in a square domain, which housed a heated rectangular obstacle; the assessment conducted revealed that at $AR = 0.1$, the Nu_{av} is invariant at the orientation of 0° and 90°. Ismael et al.[12] analyzed mixed convective flow in a porous domain containing two spinning cylinders. The study revealed that the local heat transfer coefficient is a direct function of *Ra*. Khajeh et al.[13] considered lid-driven convective heat transfer of Al_2O_3 on elliptical configurations with entropy generation incorporated. They showed that in the presence of irreversibility, heat transfer augmentation was achieved. Saieed et al.[14] numerically investigated an inclined circular enclosure driven by buoyancy in the existence of an elliptic heat source. It was reported that at high *Ra* values, the heat transfer rates improved as the inner cylinder inclination angle increased. The influence of internal heat-generating elliptic block in a porous lid-propelled square domain was examined by Bhuiyan and Munshi.[15] For high values of Darcy and Grashof numbers, it was observed that streamlines and isotherms were completely dispersed throughout the domain.

Alam et al.[16] evaluated mixed convective flow in a cavity that was exposed to Joule heating. The study shows that as the *Ra* increases, the local heat transfer coefficient amplifies. Chamkha et al.[17] examined mixed convective flow under the influence of a magnetic field and entropy generation effects of nanofluid in a porous enclosure. The investigation showed that the heat transport strength

was found to reduce with magnetic field improvement. The work of Mahfoud et al.[18] analyzed the impacts of MHD on the thermal and flow profiles within coaxial cylinders that have been heated from the bottom. Hu[19] used the lattice Boltzmann approach to study the impact of the movement of an elliptical particle in a square enclosure propelled by the lid. It was reported that the vortex location within the enclosure relies on *Re* and that the elliptical particle inertia-imposed circle limits its motion profile. Chamkha[20] considered the convective flow of fluid in a vertical lid-driven enclosure under MHD mode with internal heat production or absorption. Heat generation/absorption parameters and strength of magnetic field effects on heat transfer enhancement were extensively discussed.

Rahman et al.[21] numerically investigated the Joule heating influence on mixed convection in an unenclosed channel under the influence of a magnetic field with the bottom wall heated by a heating element. Their findings revealed that the Joule heating parameter could be utilized to adjust the thermal and flow profiles when the Rayleigh number is high. Mondal et al.[22] evaluated partial wall motion influence in a permeable cavity containing Cu–H_2O nanofluid with a heating element positioned at the center. It was theorized that the heat transfer increased crucially for higher Richardson number and high nanofluid volume fractions. Alam et al.[23] reviewed the *Ra* influence on mixed convection in a square geometry having an undulating wall. Rajarathinam et al.[24] investigated the thermal characteristics in an oriented porous cavity containing Cu–H_2O nanofluid. They found that the thermal profile improved with Darcy number and volume fraction of nanofluid. Nosonov and Sheremet[25] in the presence of a local heater considered mixed convective fluid flow in a rectangular domain. It was revealed that growth in Richardson number resulted in forced flow deformation.

El Moutaouakil et al.[26] employed the lattice Boltzmann approach to simulate buoyancy flow around a cylinder of hexagonal cross-section located in a square configuration. It was reported that the number of convective cells formed is governed by the size of the hexagon and Rayleigh number. Soomro et al.[27] explored MHD mixed convection in a triangular domain having a circular barrier. Both the thermal and fluid profiles were found to be a function of wall motion and the barrier situated in the enclosure. Taamneh and Bataineh[28] analyzed the thermal characteristics in a square cavity containing Al_2O_3–H_2O nanofluid and driven by the lid. The study shows that nanoparticle addition to base fluid improved the thermal profile of the flow. Xiong et al.[29] analyzed obstacle location influence on thermal and fluid flow characteristics in a triangular domain; it was opined that Richardson number improvement amplified the rate of transfer of heat. Moreover, Al-Farhany and Abdulsahib[30] in a two-layered nanofluid and saturated porous media considered mixed convective flow in a square domain containing an inner cylinder, which is subjected to rotary motion. The study demonstrated that the Nusselt number improved with Rayleigh number improvement. Similar results were reported for a previous study by Abdulsahib and Al-Farhany[31] for high Darcy numbers. Deb et al.[32] numerically analyzed a lid-driven cavity housing an elliptical barrier subjected to Joule heating. Adekeye et al.[33] simulated the effects of both fluid properties and some selected geometrical parameters on magnetohydrodynamic convective flow in a tilted porous elliptical enclosure exposed to localized heating. It was opined that the flow circulation decreased with growth in Hartmann number. Toghraie and Shirani[34] simulated lid-driven convective flow occurring in a cavity. It was a deduction that Richardson number improvement enhanced heat transfer. Das et al.[35] reviewed the strategies that have been employed by researchers to augment heat transfer in both forced and mixed convective heat transfer scenarios in different geometries. Padhi et al.[36] analyzed mixed convective flow in a cavity with regard to the formation of eddies. It was established that magnetic field strength improvement resulted in the velocity profiles being subdued thus giving rise to recirculation sections. Alomari et al.[37] analyzed MHD impacts on a trapezoidal cavity containing a hybrid nanofluid. The trapezium was exposed to sinusoidal heating

from below. In the study, Nu_{av} improved directly with both Ra and hybrid volume fraction improvement, but inversely with the Ha. Venkatadri et al.[38] considered mixed convective flow in a square domain having its left vertical wall subjected to central heating. Recently, Ali et al.[39] numerically studied MHD effects on mixed convection in a double lid-driven square-cavity with a cylinder obstacle. The finite element method with non-Newtonian Casson fluid has been used in their study. Two different cases have been studied depending on the cold right wall movement direction. The results showed that the rate of heat transfer was found to be the highest in Case 2 (the lid walls move in the opposite direction) compared with Case 1 at the same condition. More investigations were made by Ali et al.[40–42] regarding using double lid-driven square-cavity with a flat plate, wavy-walled enclosure, and alternated baffles with hydromagnetic effects.

Based on the literature search conducted, the uniqueness of the current work is that mixed magnetoconvection in a square enclosure equipped with internal heat generation or absorption modes and containing an adiabatic elliptic cylinder has not been considered previously. This investigation contributes to heat transfer augmentation without accruing extra energy and materials, particularly for low Re flow regimes. In addition, the heat transfer profile of the current investigation underpins the import of dimensionless numbers, such as Hartmann number, adiabatic barrier aspect ratio (AR), and heat generation/absorption parameter on the mechanism of transport of laminar combined convection in shear and buoyancy-driven enclosure. The current study finds practical significance in microelectronic devices, solar and nuclear reactor technologies, and geothermal energy systems among others.

2 | METHODOLOGY

2.1 | Description of the physical model

Figure 1 illustrates a two-dimensional representation of the physical model employed for the current investigation. The model consists of an elliptic cylinder centered in a square enclosure with an AR of $\frac{a}{b}$; where a is the length of the major axis and b is the minor axis of the ellipse. The space created by the elliptic cylinder and the enclosure is filled with a heat-conducting or absorbing fluid subjected to magnetic influence. The enclosure's flow is taken to be laminar and driven by a mixed convective mechanism. The walls of the elliptic cylinder and the horizontal boundaries of the domain are insulated. The left and right boundaries of the model are sustained at fixed thermal values of T_h and T_c, respectively. The density changes were accounted for by the Boussinesq model, and fluid properties are assumed constant. No-slip velocity was imposed on all the walls except the left vertical wall, which was assumed as a lid-driven wall.

2.2 | Governing equations

The equations of interest in dimensionless forms are as follows:

Continuity[16,21]:

$$\frac{\partial U}{\partial X} + \frac{\partial V}{\partial Y} = 0. \tag{1}$$

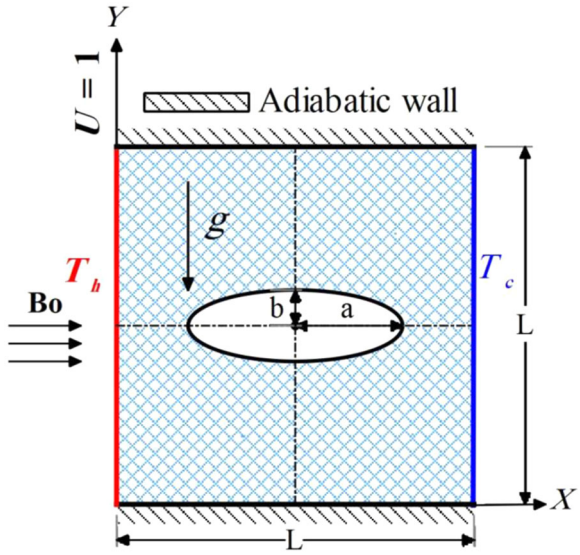


FIGURE 1 Geometry [Color figure can be viewed at wileyonlinelibrary.com]

Momentum transport equations:
X-direction:

$$U\frac{\partial U}{\partial X}+V\frac{\partial U}{\partial Y}=-\frac{\partial P}{\partial X}+\frac{1}{Re}\left[\frac{\partial^2 U}{\partial X^2}+\frac{\partial^2 U}{\partial Y^2}\right]. \tag{2}$$

Y-direction:

$$U\frac{\partial V}{\partial X}+V\frac{\partial V}{\partial Y}=-\frac{\partial P}{\partial Y}+\frac{1}{Re}\left[\frac{\partial^2 V}{\partial X^2}+\frac{\partial^2 V}{\partial Y^2}\right]+\frac{Ra}{Re^2\,Pr}\varphi-\frac{Ha^2}{Re}V. \tag{3}$$

Energy transport equation:

$$U\frac{\partial \varphi}{\partial X}+V\frac{\partial \varphi}{\partial Y}=\frac{1}{RePr}\left(\frac{\partial^2 \varphi}{\partial X^2}+\frac{\partial^2 \varphi}{\partial Y^2}\right)+\frac{J}{RePr}. \tag{4}$$

Transformation parameters

$$\begin{aligned}&X=\tfrac{x}{L},\ Y=\tfrac{y}{L},\ U=\tfrac{u}{U_0},\ V=\tfrac{v}{U_0},\\&\varphi=\tfrac{T-T_c}{T_h-T_c},\ P=\tfrac{p}{\rho u_0^2},\ Pr=\tfrac{\upsilon}{\alpha},\ J=\tfrac{Q_0L^2}{\alpha\rho c_p},\\&Ra=\tfrac{\rho g\beta(T_h-T_c)L^3}{\mu\alpha},\ Re=\tfrac{U_0L}{\upsilon},\ Ha=B_0L\sqrt{\tfrac{\sigma}{\rho\upsilon}}.\end{aligned} \tag{5}$$

2.3 | Modeling procedure

COMSOL 5.6 Multiphysics software was employed for the current investigation. The heat transfer and fluid flow settings in COMSOL Multiphysics were employed to simulate the problem. The generation was achieved by employing the free quadrilateral mesh using different parameters, such as AR, Ha, J, Re, and Gr. The meshed computational domain was approximated with the $P_1 + P_2$ interpolation function while the temperature field was discretized by Galerkin's method. To circumvent the requirement of having to stabilize the convective term in momentum equations, the meshes used were finely resolved. Local numerical instabilities were resolved by adding artificial diffusion via the streamline upwind Petrov–Galerkin's method and the segregated parametric solver was used for the thermal and flow characteristics variables. Biconjugate gradient stabilized iterative method solver was employed for the thermal and fluid flow modules of the commercial software used.[43]

3 | NUSSELT NUMBER EVALUATION

The heat transfer along the solid vertical boundaries is calculated by following Radhi[44], hence the local and mean Nusselt numbers are expressed, respectively, as:

$$Nu_L = -k\frac{\partial \varphi}{\partial X}, \tag{6}$$

$$\bar{Nu} = \frac{1}{L}\int_0^L Nu_L dY. \tag{7}$$

4 | STREAM FUNCTION

The flow motion of the fluid within the annulus of the geometry analyzed is delineated using stream function (Ψ) and it is defined from the velocity components U and V as follows[45,46]:

$$U = \frac{\partial \Psi}{\partial Y}, V = -\frac{\partial \Psi}{\partial X}. \tag{8}$$

While the stream function equation is defined by Equation (9):

$$\frac{\partial^2 \Psi}{\partial X^2} + \frac{\partial^2 \Psi}{\partial Y^2} = \frac{\partial U}{\partial Y} - \frac{\partial V}{\partial X}. \tag{9}$$

5 | VALIDATION

The integrity of the mesh quality selected was verified by carrying out grid independence examinations for various mesh sizes on $\bar{Nu}$ of the vertical lid-driven wall as displayed in Table 1. As a trade-off between the costs of computing, numerical stability, and enhanced

TABLE 1 Grid independence test of $\bar{Nu}$ on the heated vertical lid-driven wall for $Gr = 10^2$, $Re = 1000$, AR = 3, $J = 0$, and $Ha = 0$

Size of mesh	Mesh elements	Mean Nusselt number	% Absolute deviation from a mean value of $\bar{Nu}$
Coarse	3228	8.15	1.092
Normal	4262	8.16	0.971
Fine	5094	8.19	0.607
Finer	6592	8.18	0.728
Extra fine	17,278	8.22	0.243
Extremely fine	61,046	8.54	3.640

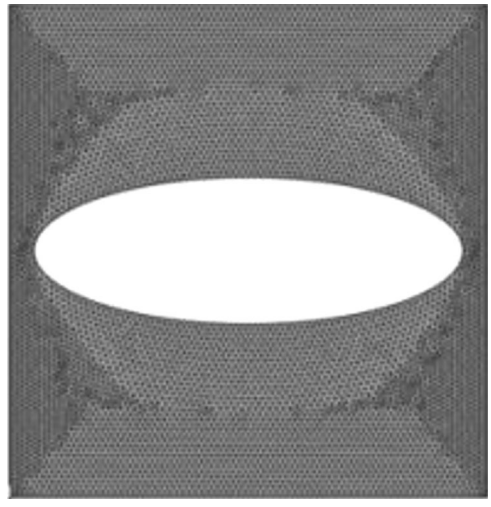


FIGURE 2 Mesh distribution

TABLE 2 Comparison of the $\bar{Nu}$ on the top wall of the cavity for $Pr = 0.71$ and $Gr = 10^2$, $Ha = 0$, $\phi = 0$ with those in literature

	Nu		
Re	**100**	**400**	**1000**
Ali et al.[40]	2.01	3.93	6.37
Khanafer and Chamkha[47]	2.01	3.91	6.33
Iwatsu et al.[48]	1.94	3.84	6.33
Present work	2.03	3.99	6.21

field resolution, extra fine mesh size was adopted for all the numerical experiments performed in this investigation as shown in Figure 2. In addition, the code used for the present study was inspected by comparing the results of the $\bar{Nu}$ gotten from the analysis of a differentially heated square enclosure whose vertical walls were subjected to

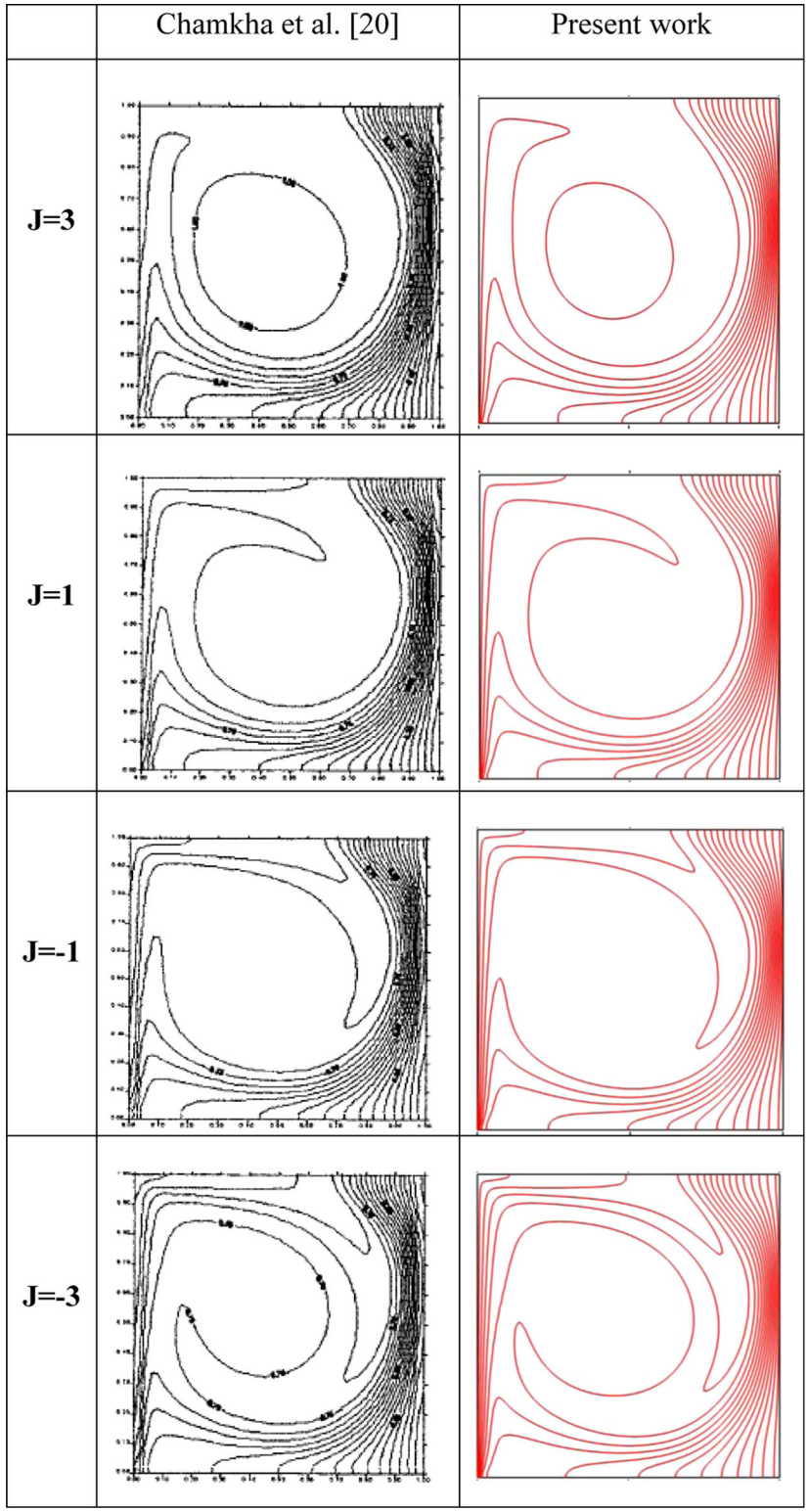


FIGURE 3 Comparison between the current study (right) with Chamkha et al.[20] study (left) in terms of the effect of the heat generation/absorption on isotherms [Color figure can be viewed at wileyonlinelibrary.com]

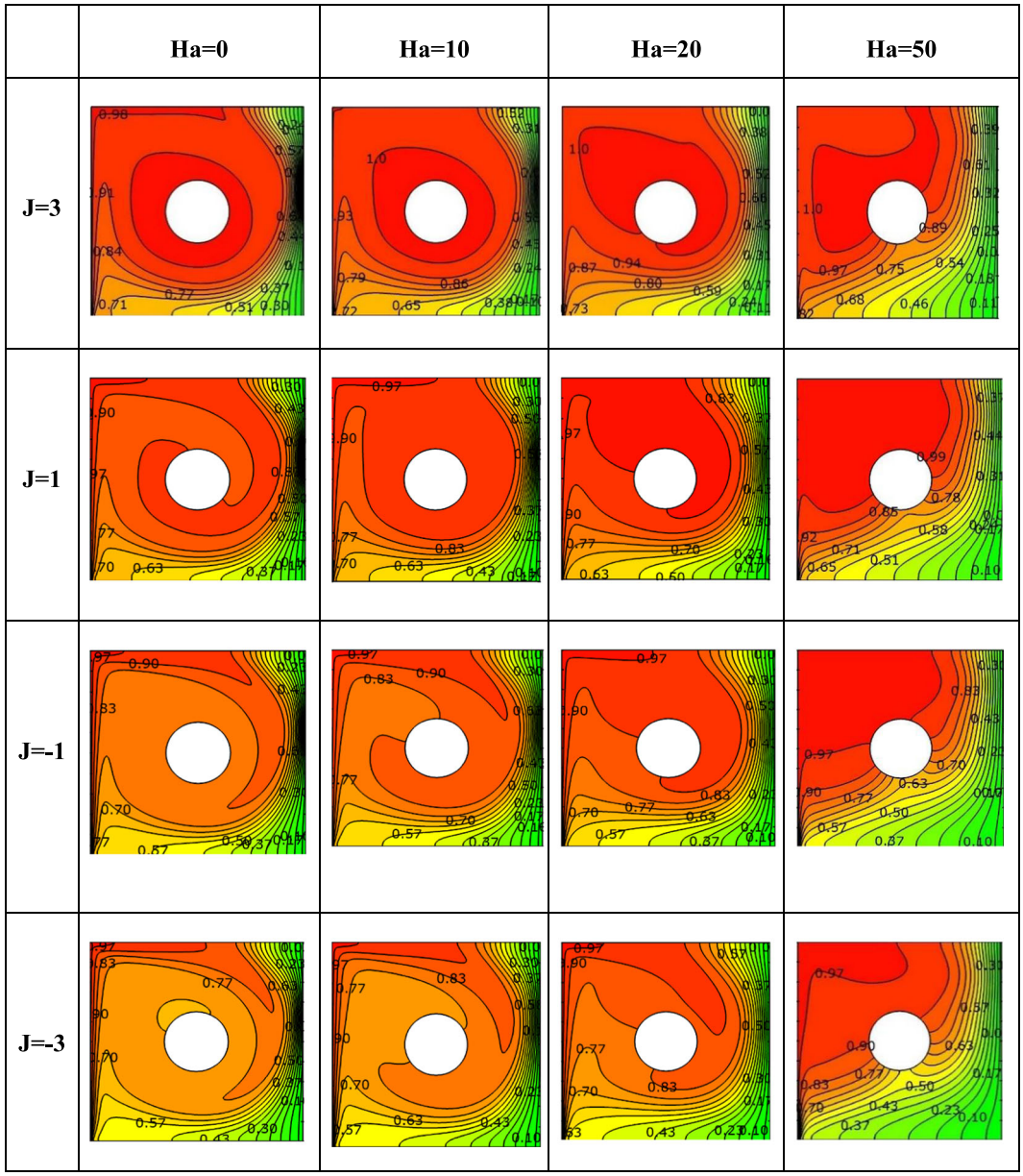


FIGURE 4 Effects of J and Ha on isothermal contours for $Gr = 100$, $Re = 1000$, and AR = 1.0 [Color figure can be viewed at wileyonlinelibrary.com]

insulation in the absence of the adiabatic cylinder with previous works under the same thermal boundary conditions. The results are delineated in Table 2 and it aligns with those of.[40,47,48] Furthermore, the response of isotherms from the current investigation to heat generation/absorption parameters are compared with those of Chamkha[20] in Figure 3 and the isotherms show good congruence.

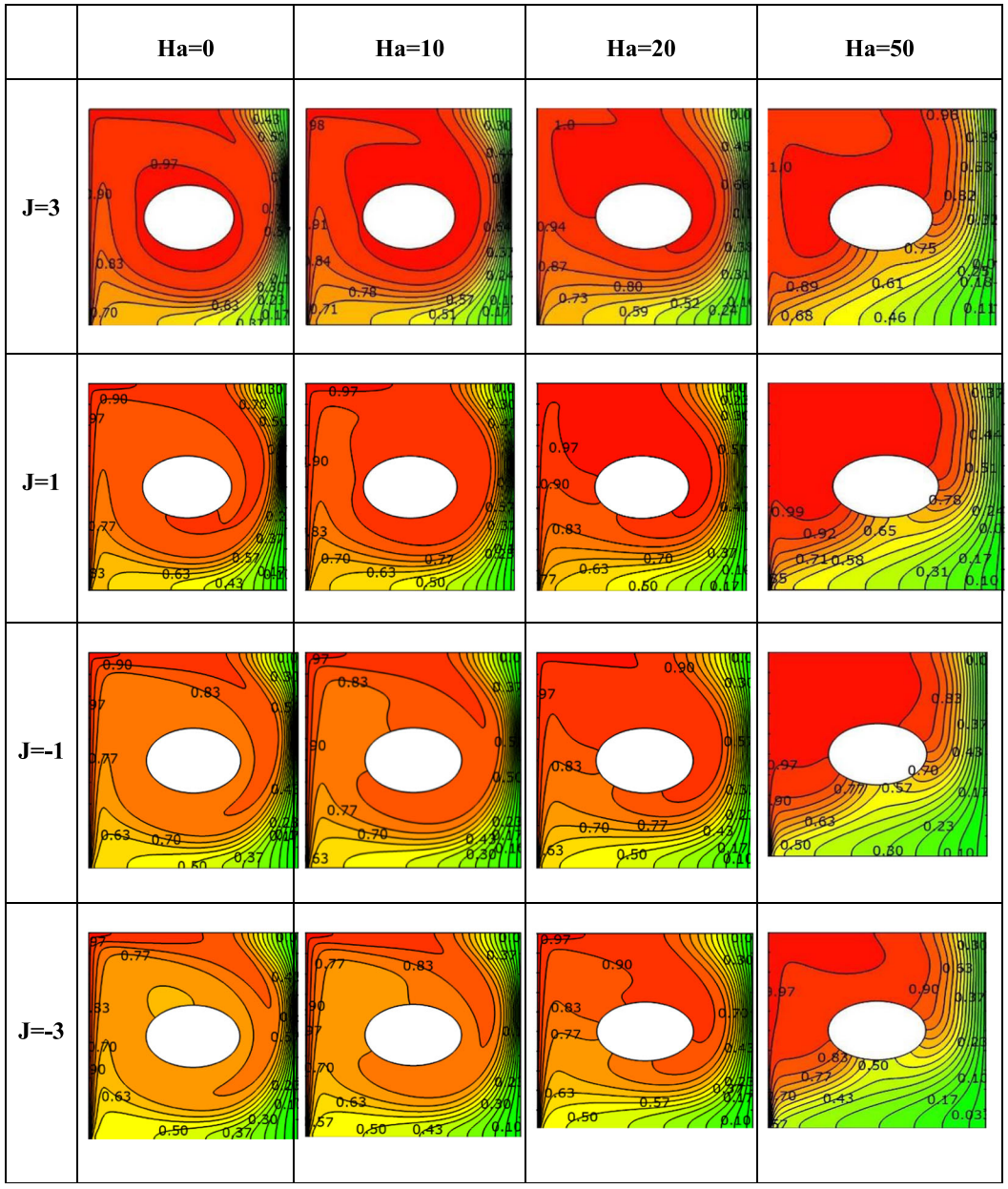


FIGURE 5 Effects of J and Ha on isothermal contours for $Gr = 100$, $Re = 1000$, and AR = 1.5 [Color figure can be viewed at wileyonlinelibrary.com]

6 | RESULTS AND DISCUSSION

Under this section, the findings for mixed convective heat transfer of fluid ($Pr = 0.71$) that is capable of generating/absorbing heat in the presence of an adiabatic elliptic obstacle positioned in a square domain under the existence of a magnetic field are presented.

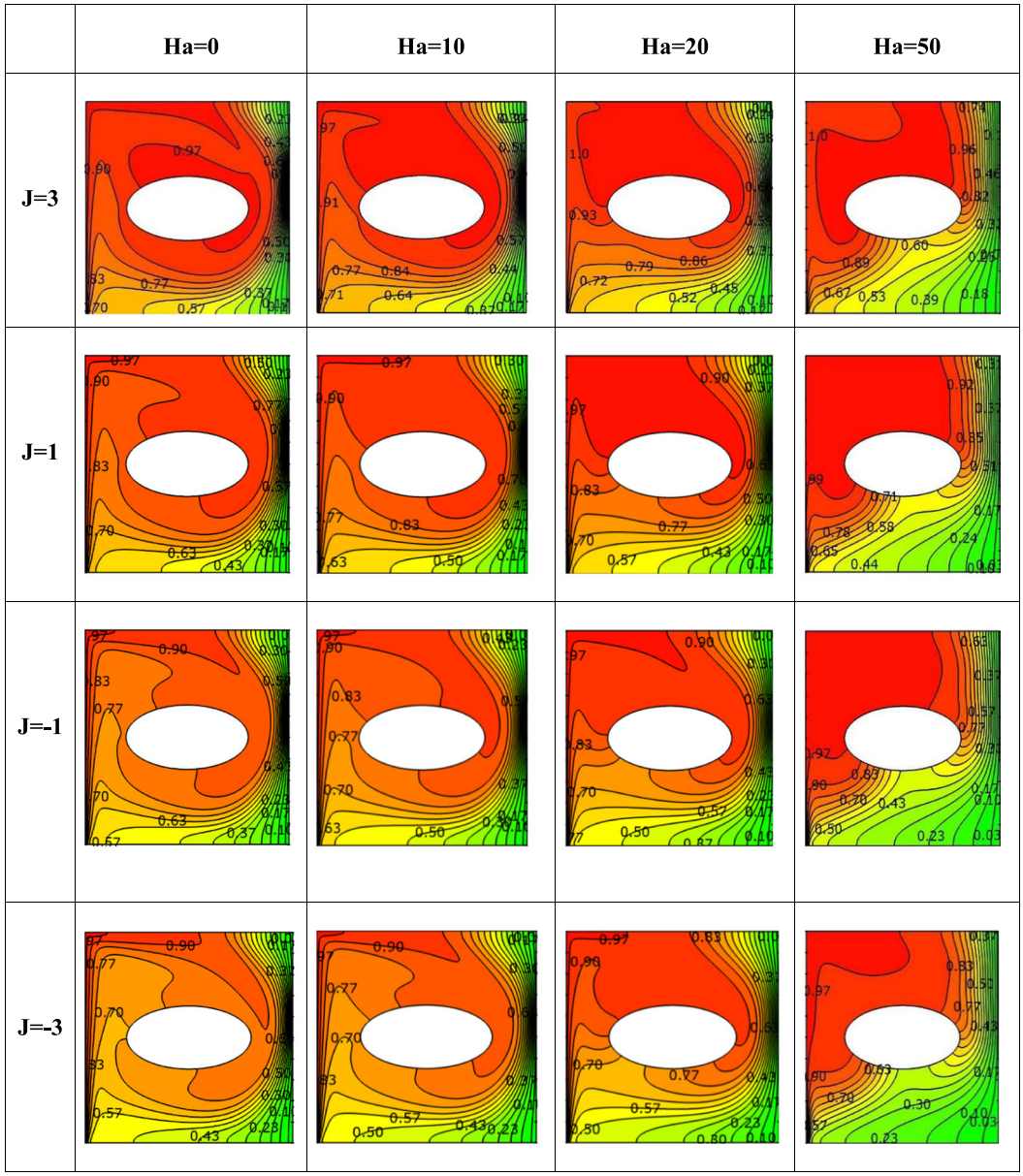


FIGURE 6 Effects of J and Ha on isothermal contours for $Gr = 100$, $Re = 1000$, and AR = 2.0 [Color figure can be viewed at wileyonlinelibrary.com]

6.1 | Effects of J, AR, and Ha on isotherm and stream function

Figures 4–8 display the isothermal plots for the present study where J varies from −3 to +3, Ha from 0 to 50, and AR from 1.0 to 3.0 while $Gr = 100$ and $Re = 1000$. The lines of isotherm near the cavity right wall are closely crowded for all cases, indicating that the temperature gradient around the right wall of the enclosure is steep. In regions that are away from the right wall of the enclosure, the gradient of temperature there is thin because the contour lines are farther

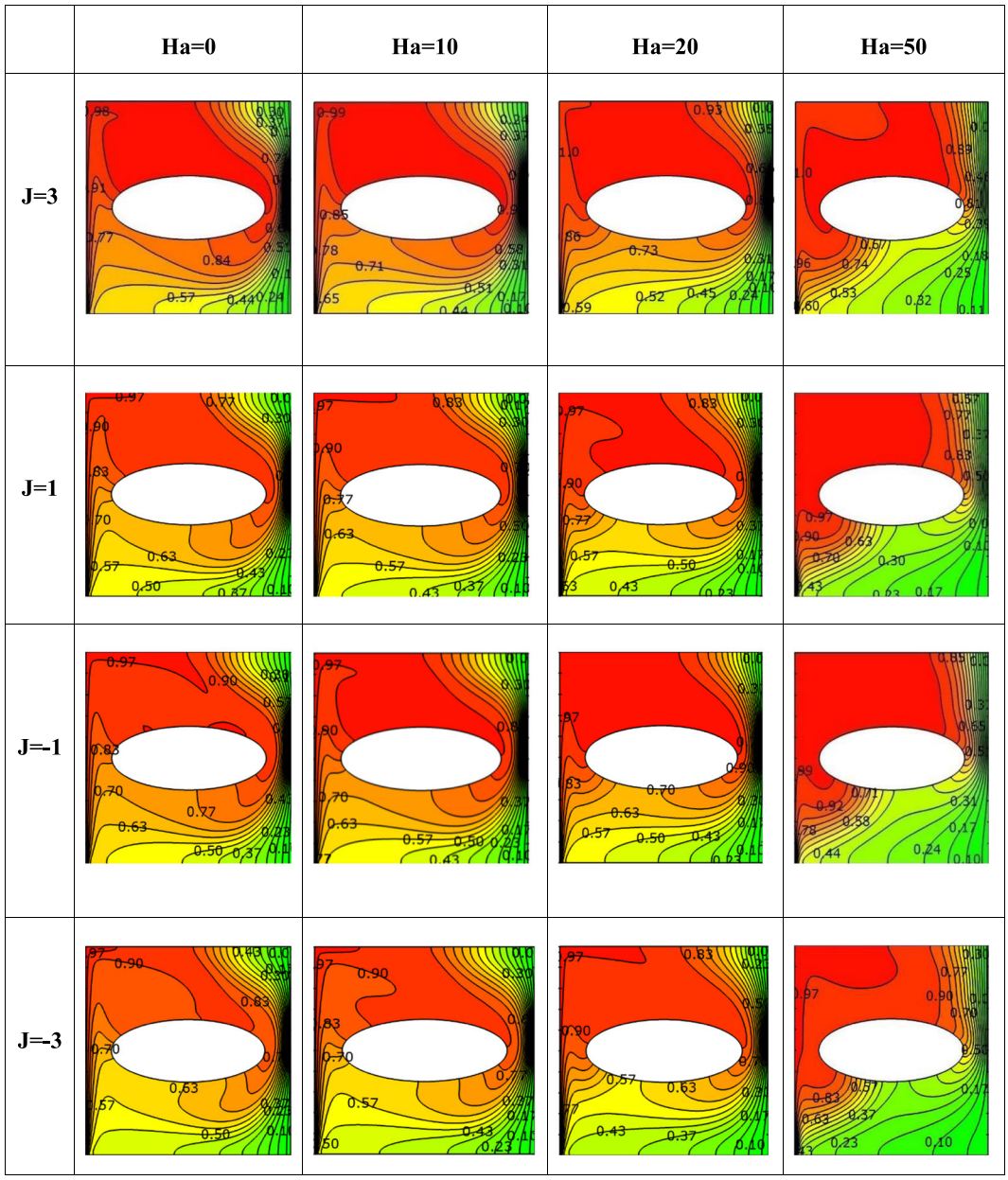


FIGURE 7 Effects of J and Ha on isothermal contours for $Gr = 100$, $Re = 1000$, and AR = 2.5 [Color figure can be viewed at wileyonlinelibrary.com]

apart; this occurrence of the steep gradient is due to the boisterous influence of the shear-driven circulations. The magnetic field influence is such that it inhibits the convective heat transfer mechanism as the isotheral lines are observed to become increasingly parallel to the wall driven by the lid; the heat transport mode in this region is largely due to conduction. When $J = 0$, the highest temperature was observed to be on the left wall but as the internal heat generation

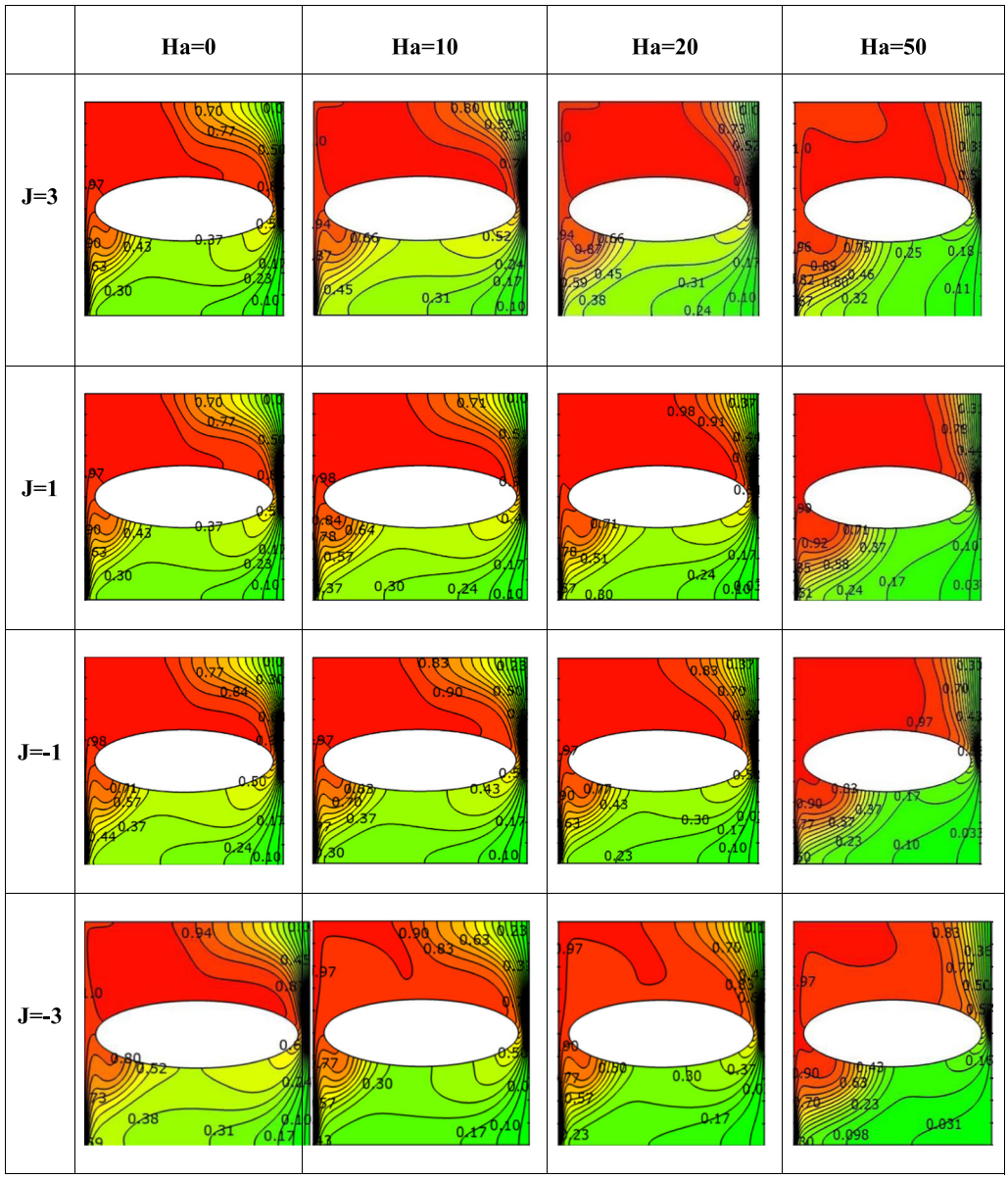


FIGURE 8 Effects of J and Ha on isothermal contours for $Gr = 100$, $\mathrm{Re} = 1000$ and $\mathrm{AR} = 3.0$ [Color figure can be viewed at wileyonlinelibrary.com]

surges ($J > 0$), the boundary layer assumes more prominence along the vertical boundaries of the enclosure with the maximum temperature drifting from the heated left wall to the isothermal contour lines immediately ahead of the diabatic cylinder; this is because the hot fluid that gets to the top insulated wall and those immediately around the adiabatic cylinder are not able to reject heat. However, for the heat absorption ($J < 0$) scenario, the maximum temperatures are observed to be very close to the hot left wall, thereby allowing for a higher heat transport rate. Also, as the magnetic influence (Ha) improves, the adjacent fluid temperatures in the enclosure around the vertical walls approximate the temperature of the

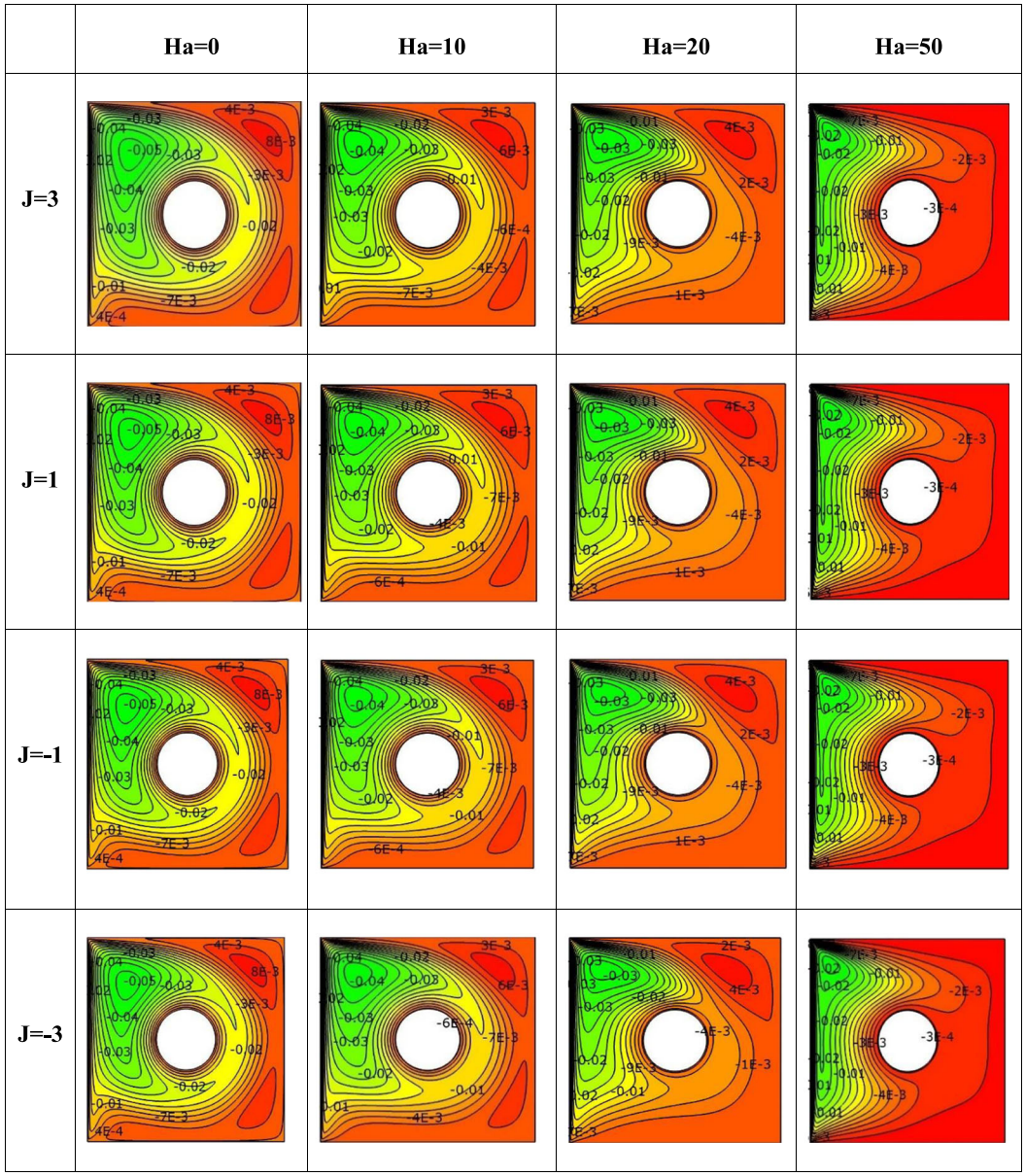


FIGURE 9 Influence of J and Ha on stream function contours for $Gr = 100$, $Re = 1000$, and AR = 1.0 [Color figure can be viewed at wileyonlinelibrary.com]

respective walls that they are close to, thereby reducing the extent of heat transfer enhancement. Finally, as the AR of the adiabatic cylinder increases, the convective force influence improved as seen in the pattern of distribution of the isothermal lines; as a consequence of this, the rate of heat transfer is enhanced.

Figures 9–13 summarize the effects of varying values of J, H, and AR on the stream function plots for $Gr = 100$ and $Re = 1000$. For all the stream function plots, the lid-driven hot left wall resulted in the clockwise rotation of main cells and anticlockwise rotation of small

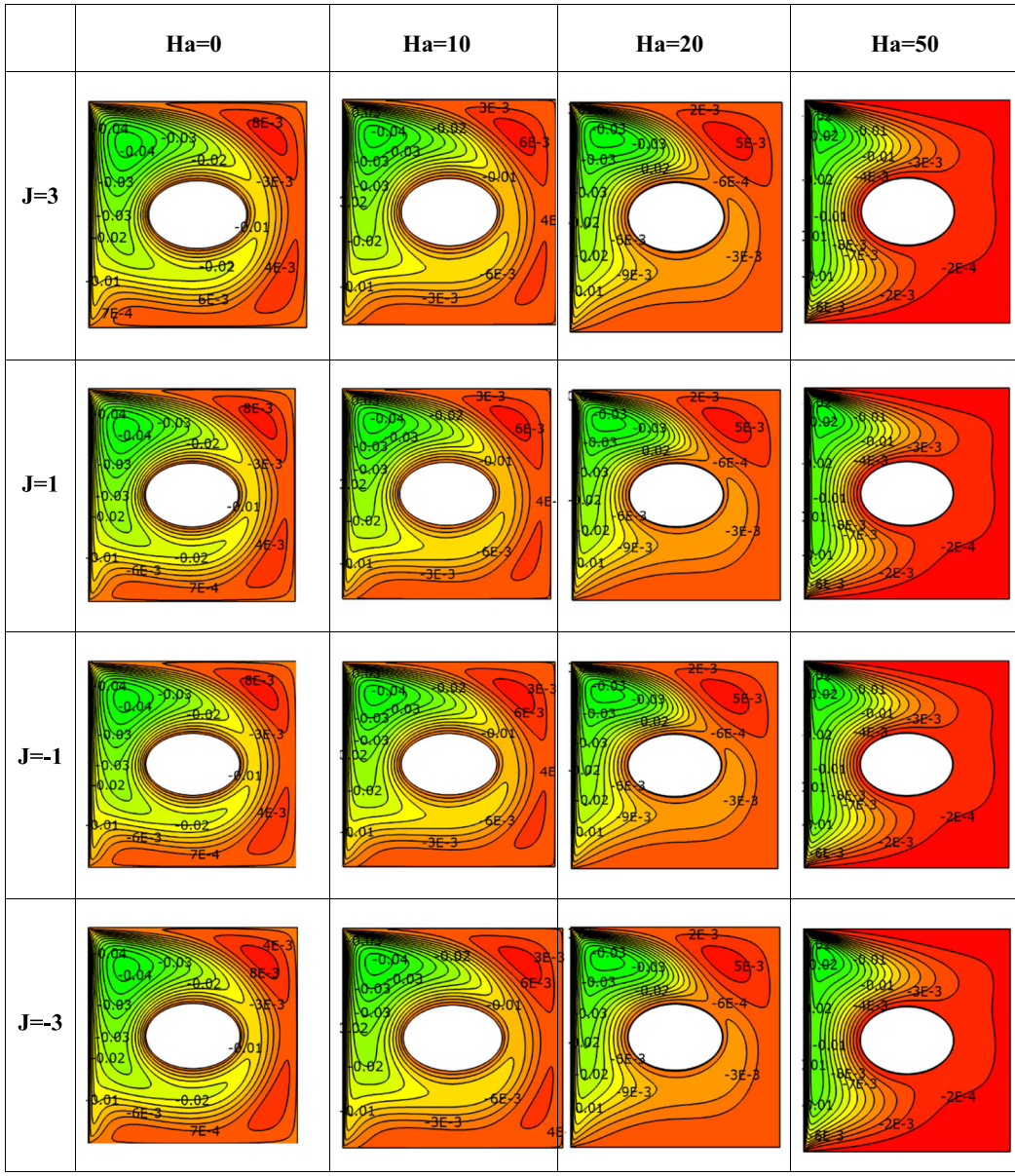


FIGURE 10 Influence of J and Ha on stream function contours for $Gr = 100$, $Re = 1000$, and AR = 1.5 [Color figure can be viewed at wileyonlinelibrary.com]

corner cells. Because the left moving wall is hot, the shear force and buoyancy force enhance the activity of the recirculation cells. Furthermore, for each of the ARs considered, the effect of a fixed value of applied magnetic force (Ha) for various J values on the stream function is negligible; this shows that Q_0 has no major consequence on the secondary flow profile. However, as Ha (strength of magnetic field) increases for a fixed value of J, the strengths of both the primary and secondary circulations decrease; this is because the Lorentz force (which is produced by the interplay of the electrically conducting flowing fluid and the

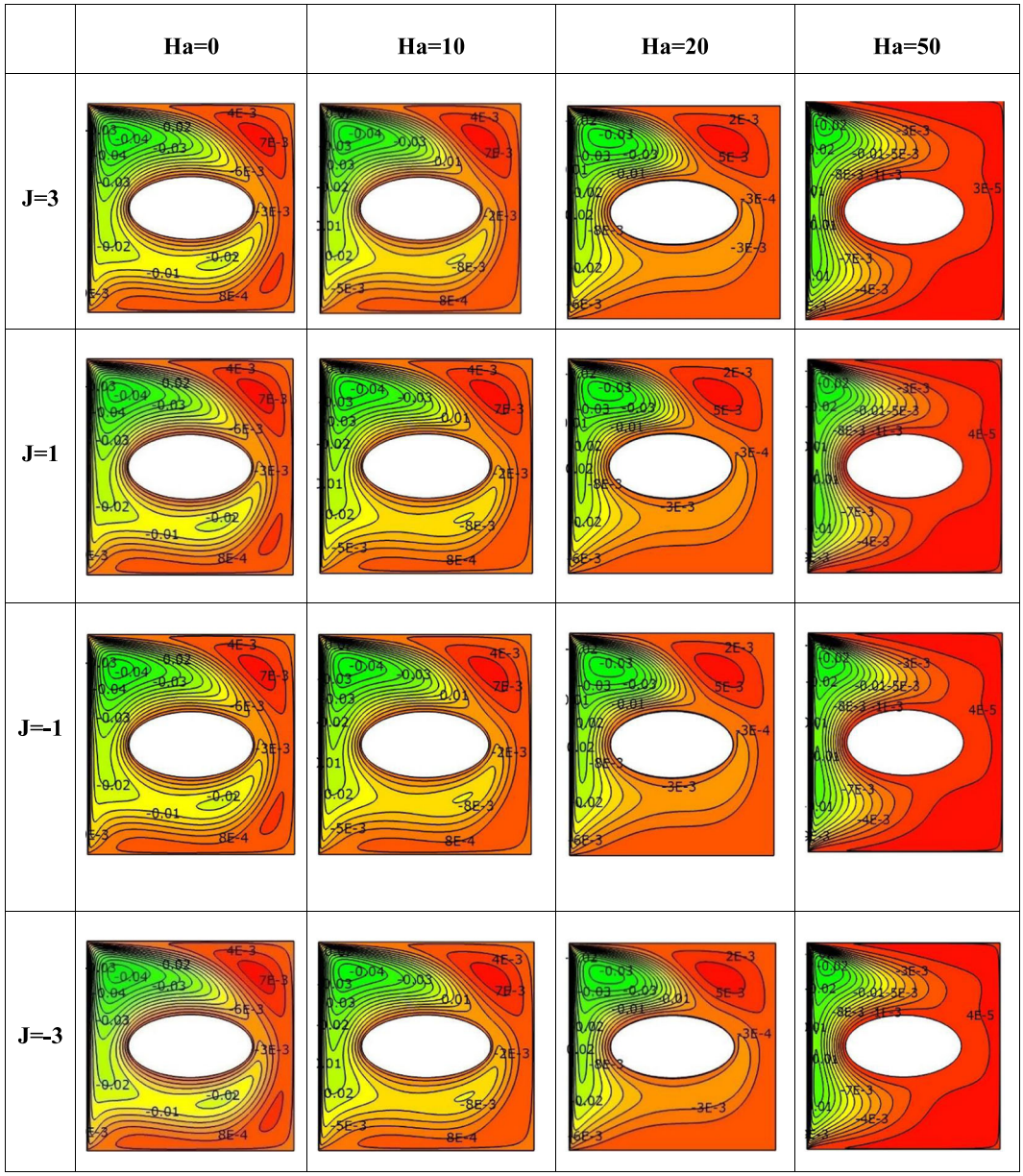


FIGURE 11 Influence of J and Ha on stream function contours for $Gr = 100$, $Re = 1000$, and AR = 2.0 [Color figure can be viewed at wileyonlinelibrary.com]

magnetic field) acts as a current inhibitor. In addition, when $Ha = 50$ for AR ≤ 2.0, the secondary circulation around the upper right corner of the square cavity vanishes as a result of further reduction in flow velocity because of the resistance offered by the magnetic force to flow. to reject heat 10, for $2.0 \leq$ AR ≤ 3.0, there is the formation of a minor cell within the main cell on the lower portion of the ellipse, which rotates in a clockwise fashion, but these soon disappear for $Ha > 10$; this could be due to the fact that an increase in Ha and AR impede flow velocity.

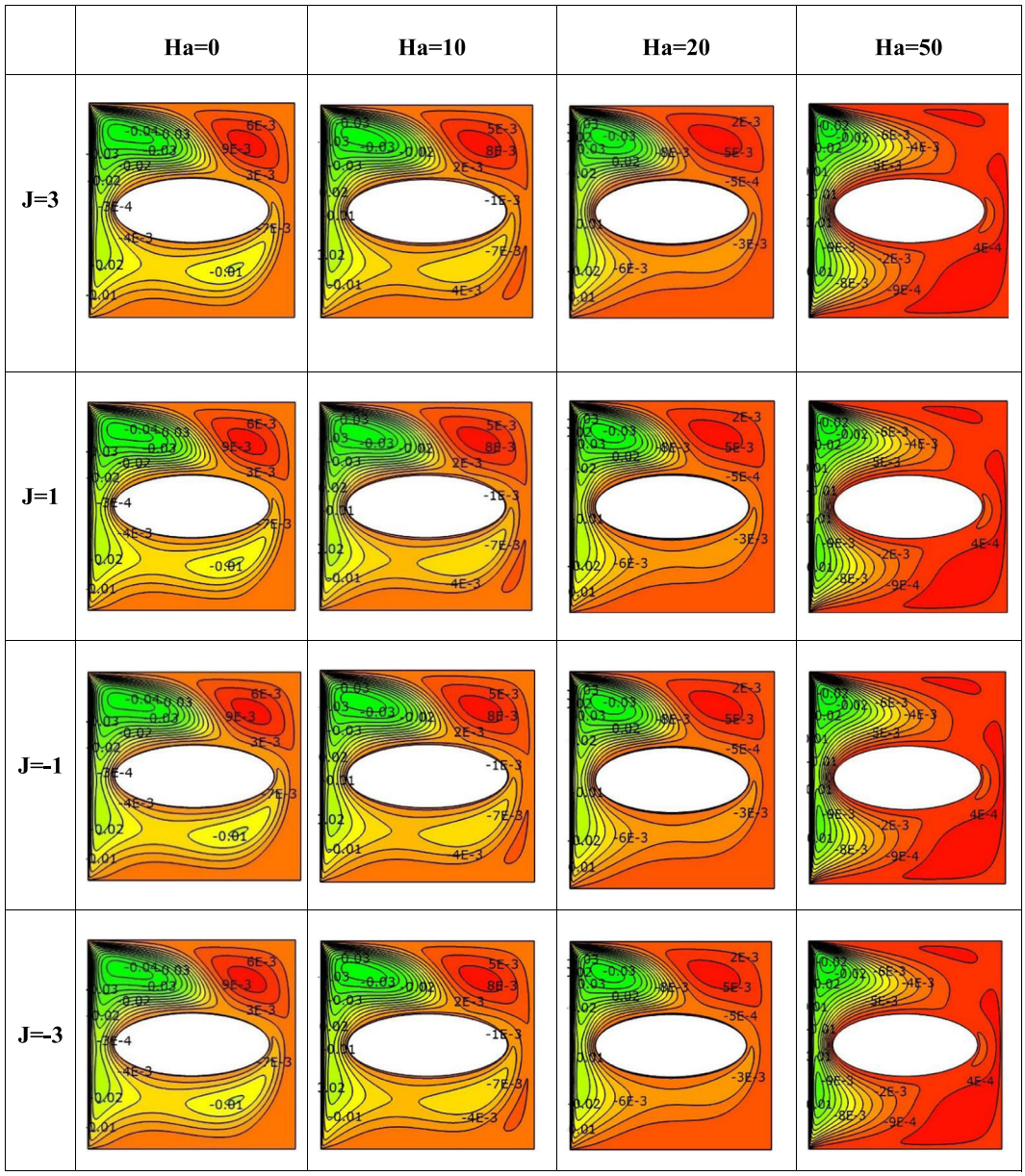


FIGURE 12 Effects of J and Ha on stream function contours for $Gr = 100$, $Re = 1000$, and AR = 2.5 [Color figure can be viewed at wileyonlinelibrary.com]

6.2 | Influence of AR on $\bar{Nu}$

Figure 14A,B delineate the plots of $\bar{Nu}$ on the hot wall against Grashof number for various ARs of the adiabatic cylinder in the absence of magnetic force ($Ha = 0$), heat sink, and heat source ($J = 0$). For all the plots, the $\bar{Nu}$ of the hot wall improves with an increase in the Grashof number. For Figure 14A, the highest heat transfer augmentation occurred when the adiabatic cylinder axis ratio is 2.0 while the least heat transfer occurred at an

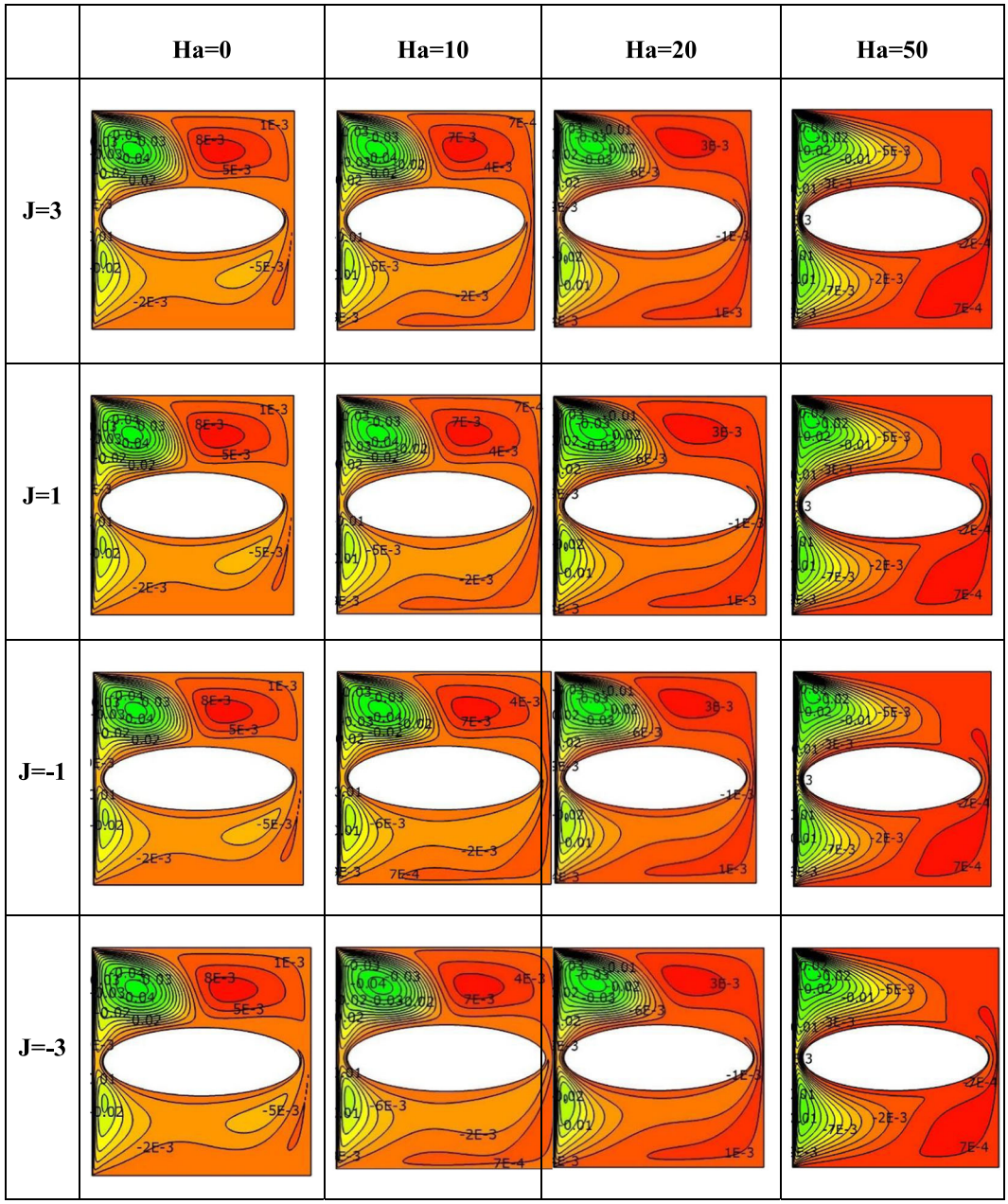


FIGURE 13 Impacts of J and Ha on stream function contours for $Gr = 100$, $Re = 1000$, and AR = 3.0 [Color figure can be viewed at wileyonlinelibrary.com]

axis ratio of 3.0. The observed trend could be because at $Re = 100$, for the range of Grashof numbers considered, convection predominates, and in addition, the temperature difference between the hot wall at AR = 3.0 and the adjoining fluid becomes marginal, hence the heat that would be transferred under this condition should reduce. However, in Figure 14B, heat transfer augmentation improves with the growth of adiabatic cylinder

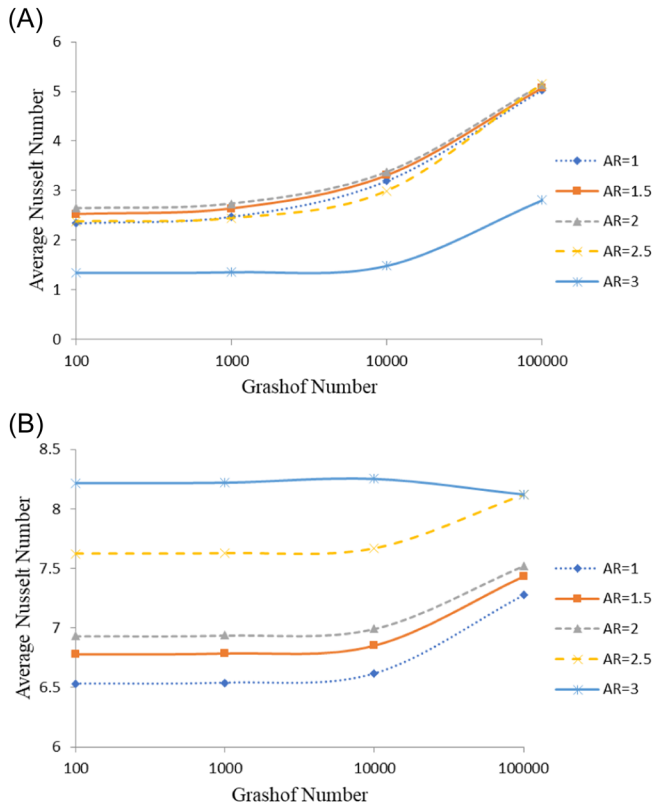


FIGURE 14 Impact of aspect ratio on Nu_{av} for (A) $Re = 100$, and (b) $Re = 1000$ when $Ha = J = 0$ [Color figure can be viewed at wileyonlinelibrary.com]

AR; this is so because force convection predominates and therefore the effect of shear force on the hot wall was able to significantly impose a wide temperature gradient between the hot wall and the adjacent fluid.

Generally speaking, when $Ha = J = 0$, that is, in the absence of magnetic field and heat-generating or absorbing influence, Richardson number ($Ri = Gr/Re^2$) dictates the relative relevance of buoyancy force as compared to shear force.

6.3 | Effect of magnetic force (Ha) on $\bar{Nu}$

The impact of the magnetic force on the heat transfer profile for various cylinder ARs in the absence of Q_0 is displayed in Figures 15 and 16. All the plots in Figures 15 and 16 reveal that Lorenz force inhibits heat transfer; this is due to the fact that Lorentz force acts as a current inhibitor. Also, at the AR of 3.0, Hartmann number increment from 0 to 10 resulted in a marginal decrease in heat transfer compared to other ranges of Hartmann numbers considered. Furthermore, higher heat transfer rates were observed in Figure 16 because of the increase in Re from 100 to 1000. This occurrence is because the increase in Re from 100 to 1000 improved the shear force of the wall driven by the lid over the effect of buoyancy force.

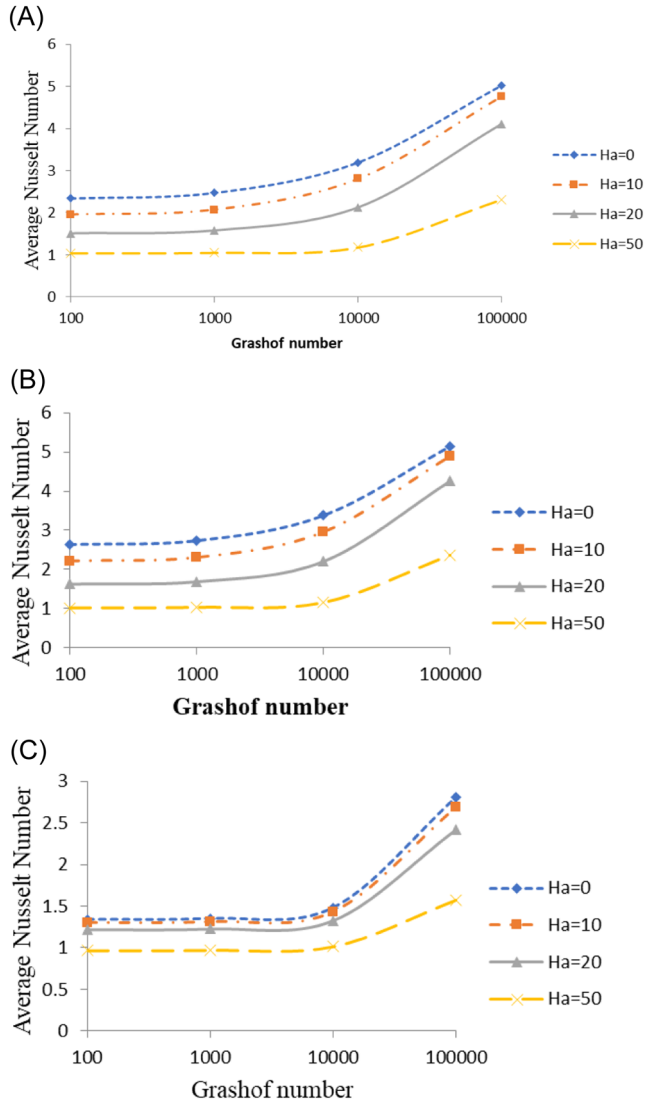


FIGURE 15 (A–C) Impact of the magnetic force on Nu_{av} for $Re = 100$, when AR = 1.0, 2.0, and 3.0 [Color figure can be viewed at wileyonlinelibrary.com]

6.4 | Influence of internal heat generation or absorption (J) on $\bar{Nu}$

The influence of J on the strength of heat transfer is presented in Figures 17 and 18 for different ARs and Reynolds numbers. The plots show that heat augmentation is favored by heat absorption and discouraged by heat generation, which is in line with the information provided by the isothermal and stream function plots above that in the vicinity of the left moving wall for the case of heat generation, the temperatures around the lid-driven wall get reduced and the fluid that gets close to the adiabatic top wall get rejected while the converse is true for heat absorption. Furthermore, the influence of AR and Reynolds

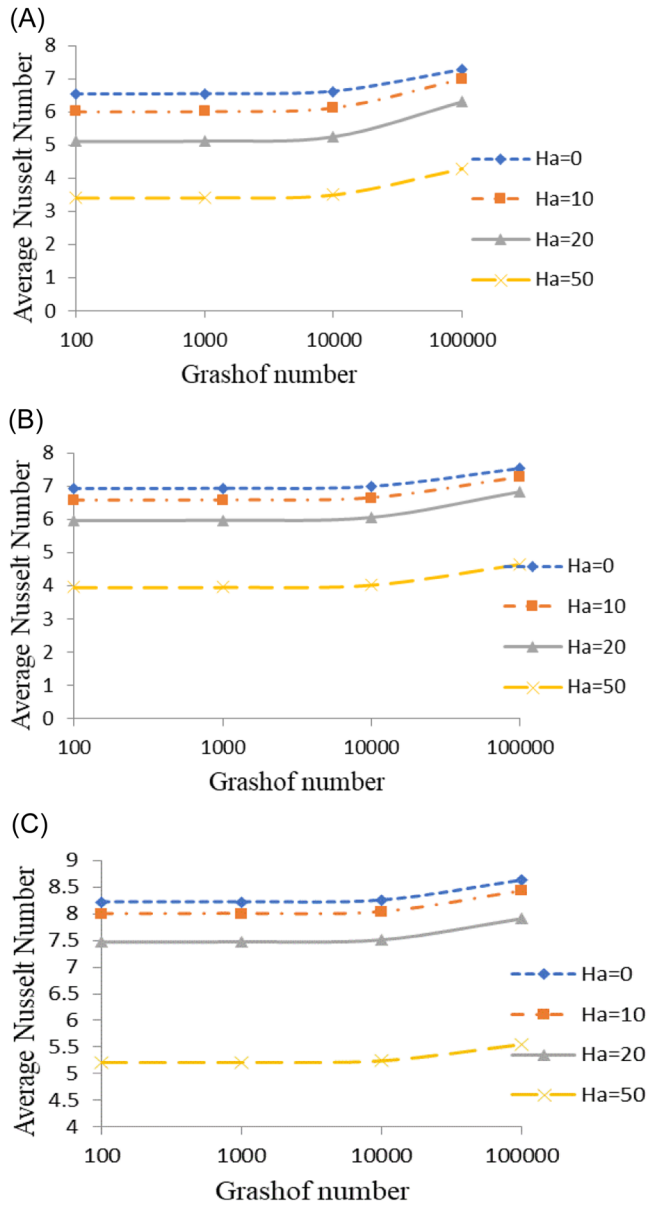


FIGURE 16 (A–C) Influence of the magnetic force on Nu_{av} for $Re = 1000$, when AR = 1.0, 2.0, and 3.0 [Color figure can be viewed at wileyonlinelibrary.com]

number variation as observed in both Figures 17 and 18 are in tandem with the information provided by Figure 14A,B, which shows that heat transfer enhancement grows with both ARs and Reynolds number improvements. Also, improvement in heat transfer in Figure 17 as compared to Figure 16 for fixed values of Grashof number ($Gr = 10^2$–10^6) as Re rises from 100 to 1000 is consistent with what is expected; this observation aligns with the report of Chamka et al.[14]

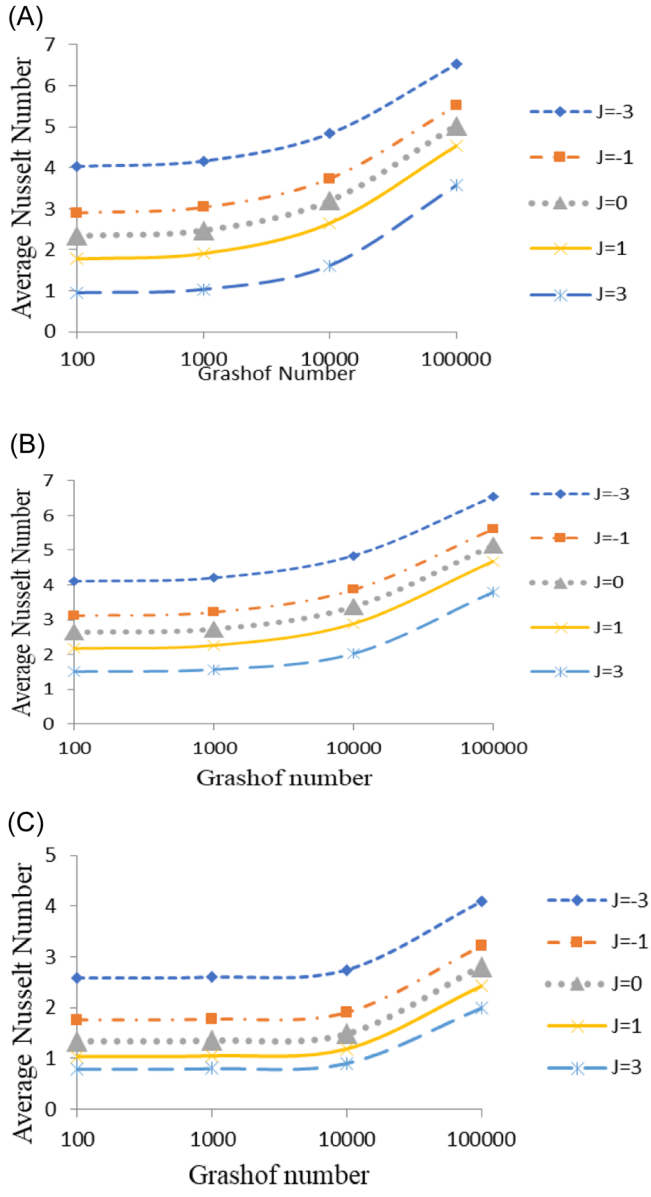


FIGURE 17 (A–C) Influence of J on average Nusselt number for $Re = 100$, when AR = 1, 2, 3 [Color figure can be viewed at wileyonlinelibrary.com]

7 | CONCLUSION

The analysis of steady laminar convective flow in a cavity driven by both shear and buoyancy forces has been performed. The cavity is filled with a fluid ($Pr = 0.71$) that has both the ability to conduct electricity and also absorb or generate heat. A numerical solution that is anchored on the method of the finite element was generated. The implications of Grashof number, Reynolds number, adiabatic cylinder AR, heat generation/absorption parameter, magnetic field on fluid flow, and heat transfer characteristics are summarized below.

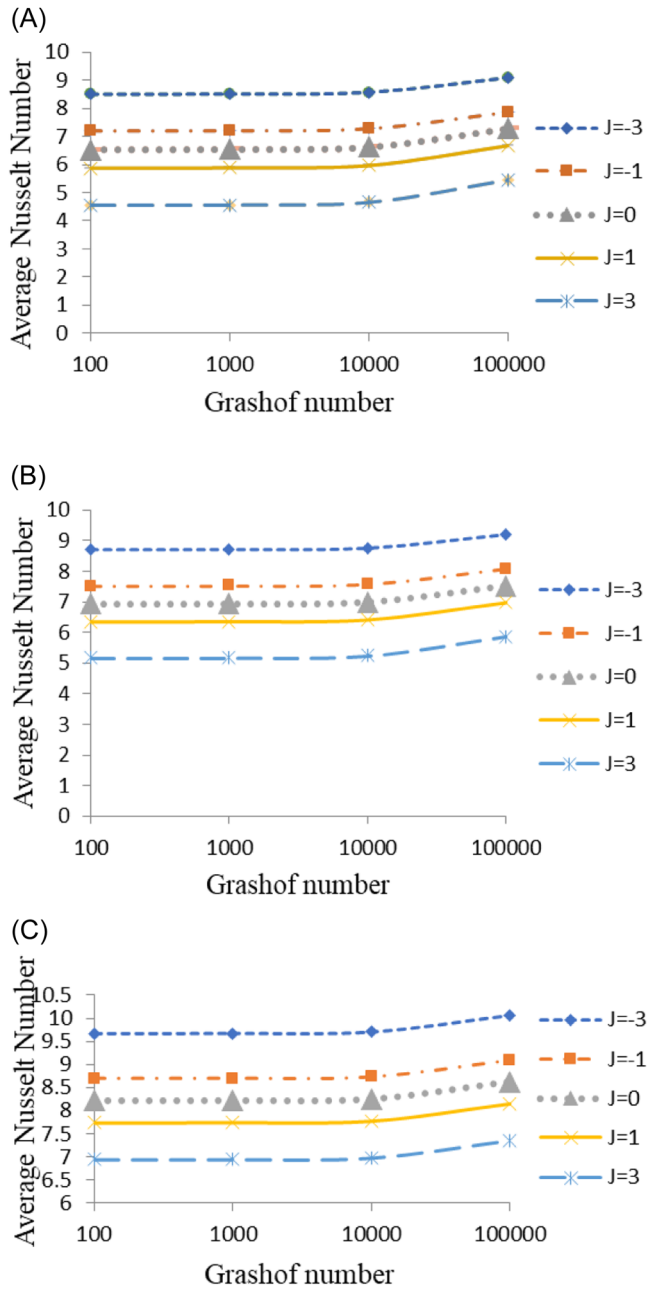


FIGURE 18 (A–C) Influence of J on average Nusselt number for $Re = 1000$, when AR = 1, 2, 3 [Color figure can be viewed at wileyonlinelibrary.com]

1. It was discovered that for Re= 100 and the range of Grashof number ($10^2 \leq Gr \leq 10^5$) considered, adiabatic cylinder gave the highest heat transfer enhancement as a further increase in AR beyond this critical value resulted in only an increase in material cost. However, when Re value was increased to 1000, the augmentation of heat transfer rises with

improvement in AR. Hence for a low Reynold number flow regime, the adiabatic cylinder AR of 2.0 is recommended as the optimum.
2. For Grashof number, AR, and Reynolds number respectively in the ranges of ($10^2 \leq Gr \leq 10^5$), ($1.0 \leq \mathrm{AR} \leq 2.0$), and ($100 \leq \mathrm{AR} \leq 1000$), Hartmann number increment resulted in heat transfer suppression; and beyond $\mathrm{AR} = 2.0$, the heat transfer rate for $Ha = 10$ approximates those transferred when the magnetic field was not considered.
3. For all the range of parameters considered, heat generation improvement declines heat transfer augmentation while heat transfer improvement is favored by the rising value of heat absorption.
4. The fluid flow and thermal history are largely affected by the size of the adiabatic elliptical cylinder.
5. For low Reynolds number flow, the impact of cylinder size on heat transfer diminishes beyond $Gr = 10^4$. But for high Reynolds ($Re = 1000$), heat transfer augmentation is aided by increasing cylinder size.

NOMENCLATURE

a	semi-major axis
AR	aspect ratio
b	semi-minor axis (m)
B_0	magnetic induction (T)
g	acceleration due to gravity (m/s^2)
Ha	Hartmann number
J	dimensionless heat generation coefficient
k	thermal conductivity (W/mK)
L	dimensionless height of the enclosure
Nu	local Nusselt number
$\bar{Nu}$	average Nusselt number
p	dimensional pressure (N/m^2)
P	dimensionless pressure
Pr	Prandtl number
Q_0	heat generation or absorption coefficient
Ra	Rayleigh number
Re	Reynolds number
T	dimensional temperature (K)
T_c	dimensional cold wall temperature (K)
T_h	dimensional hot wall temperature (K)
u, v	dimensional velocity components (m/s)
U, V	dimensionless velocity components
x, y	dimensional Cartesian coordinates (m)
X, Y	dimensionless Cartesian coordinates

GREEK SYMBOLS

α	thermal diffusivity (m^2/s)
ν	kinematic Viscosity (m^2/s)
σ	electrical conductivity (S/m)
ρ	density (kg/m^3)

φ dimensionless temperature
Ψ dimensionless stream function

DATA AVAILABILITY STATEMENT

The data that support the findings of this study are available from the corresponding author upon reasonable request.

ORCID

Khaled Al-Farhany http://orcid.org/0000-0002-5806-3800
Adebowale M. Obalalu http://orcid.org/0000-0002-7597-0525

REFERENCES

1. Abdulsahib AD, Al-Farhany K. Review of the effects of stationary/rotating cylinder in a cavity on the convection heat transfer in porous media with/without nanofluid. *Math Model Eng Probl*. 2021;8(3):356-364. doi:10.18280/mmep.080304
2. Al-Chlaihawi KK, Alaydamee HH, Faisal AE, Al-Farhany K, Alomari MA. Newtonian and non-Newtonian nanofluids with entropy generation in conjugate natural convection of hybrid nanofluid-porous enclosures: a review. *Heat Transfer*. 2022;51(2):1725-1745. doi:10.1002/htj.22372
3. Abdulkadhim A, Abed IM, Said NM. An exhaustive review on natural convection within complex enclosures: Influence of various parameters. *Chin J Phys*. 2021;74:365-388. doi:10.1016/j.cjph.2021.10.012
4. Abdulkadhim A, Abed IM, Mahjoub Said N. Review of natural convection within various shapes of enclosures. *Arab J Sci Eng*. 2021;46(12):11543-11586. doi:10.1007/s13369-021-05952-6
5. Redouane F, Jamshed W, Devi SSU, et al. Influence of entropy on Brinkman–Forchheimer model of MHD hybrid nanofluid flowing in enclosure containing rotating cylinder and undulating porous stratum. *Sci Rep*. 2021;11(1):24316. doi:10.1038/s41598-021-03477-4
6. Al-Farhany K, Alomari MA, Al-Saadi A, Chamkha A, Öztop HF, Al-Kouz W. MHD mixed convection of a Cu–water nanofluid flow through a channel with an open trapezoidal cavity and an elliptical obstacle. *Heat Transfer*. 2022;51(2):1691-1710. doi:10.1002/htj.22370
7. Olayemi OA, Al-Farhany K, Olaogun O, Ibiwoye MO, Medupin RO, Jinadu A. Computational fluid dynamics analysis of mixed convection heat transfer and fluid flow in a lid-driven square cavity subjected to different heating conditions. *IOP Conf Ser Mater Sci Eng*. 2021;1107(1):012201. doi:10.1088/1757-899x/1107/1/012201
8. Khan M, Khan AA, Hasan MN. Numerical study of mixed convection heat transfer from a rotating cylinder inside a trapezoidal enclosure. *AIP Conf Proc*. 2016;1754:050036. doi:10.1063/1.4958427
9. Yang L, Farouk B. Mixed convection around a heated rotating horizontal square cylinder in a circular enclosure. *Numer Heat Transfer*. 1995;28(1):1-18. doi:10.1080/10407789508913729
10. Chamkha AJ, Selimefendigil F, Ismael MA. Mixed convection in a partially layered porous cavity with an inner rotating cylinder. *Numer Heat Transfer*. 2016;69(6):659-675. doi:10.1080/10407782.2015.1081027
11. Olayemi OA, Khaled AF, Temitope OJ, Victor OO, Odetunde CB, Adegun IK. Parametric study of natural convection heat transfer from an inclined rectangular cylinder embedded in a square enclosure. *Aust J Mech Eng*. 2021. doi:10.1080/14484846.2021.1913853
12. Ismael MA, Selimefendigil F, Chamkha AJ. Mixed convection in a vertically layered fluid-porous medium enclosure with two inner rotating cylinders. *J Porous Media*. 2017;20(6):491-511. doi:10.1615/JPorMedia.v20.i6.20
13. Khajeh K, Jahanshaloo L, Ebrahimi S, Aminfar H. Mixed convection heat transfer of Al_2O_3 nanofluid on the elliptical shapes: numerical study of irreversibility. *J Appl Fluid Mech*. 2018;11(1):177-189. doi:10.29252/jafm.11.01.28080
14. Saieed ANA, Al-Mousawe STM, Abtan AA, Habeeb LJ. Bouyancy driven in an inclind circular enclosure with elliptic heat source. *J Mech Eng Res Dev*. 2020;43(7):62-74.
15. Bhuiyan AH, Munshi MJH. Hydrodynamic mixed convection in a lid-driven porous square cavity with internal heat generating elliptic block. *GANIT J Bangladesh Math Soc*. 2018;37:175-183. doi:10.3329/ganit.v37i0.35735

16. Alam MS, Alim MA, Mollah MSH. Mixed magneto convection in a lid driven square enclosure with a sinusoidal vertical wall and Joule heating. *Procedia Eng*. 2017;194:463-470. doi:10.1016/j.proeng.2017.08.172
17. Chamkha AJ, Mansour MA, Rashad AM, Kargarsharifabad H, Armaghani T. Magnetohydrodynamic mixed convection and entropy analysis of nanofluid in gamma-shaped porous cavity. *J Thermophys Heat Transfer*. 2020;34(4):836-847. doi:10.2514/1.T5983
18. Mahfoud B, Benhacine H, Laouari A, Bendjaghlouli A. Magnetohydrodynamic effect on flow structures between coaxial cylinders heated from below. *J Thermophys Heat Transfer*. 2020;34(2):265-274. doi:10.2514/1.T5805
19. Hu J. Motion of a neutrally buoyant elliptical particle in a lid-driven square cavity. *Eur J Mech*. 2021;85: 124-133. doi:10.1016/j.euromechflu.2020.09.008
20. Chamkha AJ. Hydromagnetic combined convection flow in a vertical lid-driven cavity with internal heat generation or absorption. *Numer Heat Transfer*. 2002;41(5):529-546. doi:10.1080/104077802753570356
21. Rahman MM, Öztop HF, Rahim NA, Saidur R, Al-Salem K. MHD mixed convection with Joule heating effect in a lid-driven cavity with a heated semi-circular source using the finite element technique. *Numer Heat Transfer*. 2011;60(6):543-560. doi:10.1080/10407782.2011.609087
22. Mondal MK, Biswas N, Sarkar UK, Manna NK, Mandal DK. Effect of partial wall motion on MHD mixed convection heat transfer undergoing in a porous cavity filled with Cu–water nanofluid with a centrally mounted heat source. *IOP Conf Ser Mater Sci Eng*. 2021;1080(1):012025. doi:10.1088/1757-899x/1080/1/012025
23. Alam MS, Mollah MSH, Alim MA, Ali MM, Munshi MJH. Effect of Rayleigh number magneto-convection in a lid driven square cavity with a sinusoidal wall. *AIP Conf Proc*. 2019;2121:030021. doi:10.1063/1.5115866
24. Rajarathinam M, Nithyadevi N, Chamkha AJ. Heat transfer enhancement of mixed convection in an inclined porous cavity using Cu-water nanofluid. *Adv Powder Technol*. 2018;29(3):590-605. doi:10.1016/j.apt.2017.11.032
25. Nosonov II, Sheremet MA. Conjugate mixed convection in a rectangular cavity with a local heater. *Int J Mech Sci*. 2018;136:243-251. doi:10.1016/j.ijmecsci.2017.12.049
26. El Moutaouakil L, Zrikem Z, Abdelbaki A. Lattice Boltzmann simulation of natural convection in an annulus between a hexagonal cylinder and a square enclosure. *Math Probl Eng*. 2017;2017:3834170. doi:10.1155/2017/3834170
27. Soomro FA, Haq RU, Algehyne EA, Tlili I. Thermal performance due to magnetohydrodynamics mixed convection flow in a triangular cavity with circular obstacle. *Journal of Energy Storage*. 2020;31:101702. doi:10.1016/j.est.2020.101702
28. Taamneh Y, Bataineh K. Mixed convection heat transfer in a square lid-driven cavity filled with Al_2O_3-Water Nanofluid. *Stroj Vestn J Mech Eng*. 2017;63(6):383-393. doi:10.5545/sv-jme.2017.4449
29. Xiong PY, Hamid A, Iqbal K, Irfan M, Khan M. Numerical simulation of mixed convection flow and heat transfer in the lid-driven triangular cavity with different obstacle configurations. *Int Commun Heat Mass Transfer*. 2021;123:105202. doi:10.1016/j.icheatmasstransfer.2021.105202
30. Al-Farhany K, Abdulsahib AD. Study of mixed convection in two layers of saturated porous medium and nanofluid with rotating circular cylinder. *Prog Nucl Energy*. 2021;135:103723. doi:10.1016/j.pnucene.2021.103723
31. Abdulsahib AD, Al-Farhany K. Numerical Investigation of the nanofluid mixed convection on two layers enclosure with rotating cylinder: high Darcy number effects. *IOP Conf Ser Mater Sci Eng*. 2020;928(2): 022001. doi:10.1088/1757-899X/928/2/022001
32. Deb D, Poudel S, Chakrabarti A. Numerical simulation of hydromagnetic convection in a lid-driven cavity containing a heat conducting elliptical obstacle with Joule heating. *Int J Eng Res Technol*. 2017;6:99-105. doi:10.17577/IJERTV6IS080055
33. Adekeye T, Adegun IK, Okekunle PO, et al. Numerical analysis of the effects of selected geometrical parameters and fluid properties on MHD natural convection flow in an inclined elliptic porous enclosure with localized heating. *Heat Transfer*. 2017;46(3):261-293. doi:10.1002/htj.21211
34. Toghraie D, Shirani E. Numerical simulation of water/alumina nanofluid mixed convection in square lid-driven cavity: effect of magnetic field using a two-phase model. *Int J Numer Methods Heat Fluid Flow*. 2020; 30(5):2781-2807. doi:10.1108/HFF-02-2019-0114
35. Das D, Roy M, Basak T. Studies on natural convection within enclosures of various (non-square) shapes—a review. *Int J Heat Mass Transfer*. 2017;106:356-406. doi:10.1016/j.ijheatmasstransfer.2016.08.034
36. Padhi P, Udhayakumar S, Sekhar TVS, Sivakumar R. Thermo-magneto-convection and mechanism of multiple eddy formation due to applied magnetic field in a lid-driven cavity. *Eng Res Express*. 2021;3(1): 015013. doi:10.1088/2631-8695/abde4d

37. Alomari MA, Al-Farhany K, Hashem AL, Al-Dawody MF, Redouane F, Olayemi OA. Numerical study of mhd natural convection in trapezoidal enclosure filled with (50% MgO-50% Ag/water) hybrid nanofluid: heated sinusoidal from below. *Int J Heat Technol*. 2021;39(4):1271-1279. doi:10.18280/ijht.390425
38. Venkatadri K, Gouse Mohiddin S, Suryanarayana Reddy M. Numerical analysis of unsteady MHD mixed convection flow in a lid-driven square cavity with central heating on left vertical wall. In: Singh M, Kushvah B, Seth G, Prakash J, eds. *Applications of Fluid Dynamics*. Singapore: Springer; 2018:355-370.
39. Ali MM, Akhter R, Alim MA. Performance of flow and heat transfer analysis of mixed convection in Casson fluid filled lid driven cavity including solid obstacle with magnetic impact. *SN Appl Sci*. 2021;3(2):250. doi:10.1007/s42452-021-04243-x
40. Ali MM, Akhter R, Alim MA. Magneto-mixed convection in a lid driven partially heated cavity equipped with nanofluid and rotating flat plate. *Alex Eng J*. 2022;61(1):257-278. doi:10.1016/j.aej.2021.05.003
41. Mokaddes Ali M, Akhter R, Alim MA. Hydromagnetic natural convection in a wavy-walled enclosure equipped with hybrid nanofluid and heat generating cylinder. *Alex Eng J*. 2021;60(6):5245-5264. doi:10.1016/j.aej.2021.04.059
42. Ali MM, Akhter R, Miah MM. Hydromagnetic mixed convective flow in a horizontal channel equipped with Cu-water nanofluid and alternated baffles. *Int J Thermofluids*. 2021;12:100118. doi:10.1016/j.ijft.2021.100118
43. Selimefendigil F, Ismael MA, Chamkha AJ. Mixed convection in superposed nanofluid and porous layers in square enclosure with inner rotating cylinder. *Int J Mech Sci*. 2017;124-125:95-108. doi:10.1016/j.ijmecsci.2017.03.007
44. Radhi ZK. Study natural convection in a porous trapezoidal cavity with a square body at the center of the enclosure. *Eng Technol J*. 2013;31(14):2632-2649.
45. Al-Farhany K, Al-Chlaihawi KK, Al-dawody MF, Biswas N, Chamkha AJ. Effects of fins on magnetohydrodynamic conjugate natural convection in a nanofluid-saturated porous inclined enclosure. *Int Commun Heat Mass Transfer*. 2021;126:105413. doi:10.1016/j.icheatmasstransfer.2021.105413
46. Al-Farhany K, Al-dawody MF, Hamzah DA, Al-Kouz W, Said Z. Numerical investigation of natural convection on Al_2O_3–water porous enclosure partially heated with two fins attached to its hot wall: under the MHD effects. *Appl Nanosci*. 2021. doi:10.1007/s13204-021-01855-y
47. Khanafer KM, Chamkha AJ. Mixed convection flow in a lid-driven enclosure filled with a fluid-saturated porous medium. *Int J Heat Mass Transfer*. 1999;42(13):2465-2481. doi:10.1016/S0017-9310(98)00227-0
48. Iwatsu R, Hyun JM, Kuwahara K. Mixed convection in a driven cavity with a stable vertical temperature gradient. *Int J Heat Mass Transfer*. 1993;36(6):1601-1608. doi:10.1016/S0017-9310(05)80069-9

How to cite this article: Olayemi OA, Al-Farhany K, Obalalu AM, Ajide TF, Adebayo KR. Magnetoconvection around an elliptic cylinder placed in a lid-driven square enclosure subjected to internal heat generation or absorption. *Heat Transfer*. 2022;1-27. doi:10.1002/htj.22530